

# A new class of galaxy models with a central BH - I. The spherical case

Luca Ciotti<sup>1</sup>, Antonio Mancino<sup>1</sup>, Silvia Pellegrini<sup>1</sup>

<sup>1</sup>*Department of Physics and Astronomy, University of Bologna, via Gobetti 93/3, 40129 Bologna, Italy*

Accepted, September 17, 2019

## ABSTRACT

The dynamical properties of spherically symmetric galaxy models, where a Jaffe (1983) stellar density profile is embedded in a total mass density decreasing as  $r^{-3}$  at large radii, are presented. The orbital structure of the stellar component is described by the Osipkov–Merritt anisotropy; the dark matter halo is isotropic, and a black hole is added at the center of the galaxy. First, the conditions for a nowhere negative and monotonically decreasing dark matter halo density profile are derived; this profile can be made asymptotically coincident with a NFW profile at the center and at large radii. Then the minimum value of the anisotropy radius for phase-space consistency is derived as a function of the galaxy parameters. The Jeans equations for the stellar component are solved analytically; the projected velocity dispersion at the center and at large radii is also obtained, for generic values of the anisotropy radius. Finally, analytical expressions for the terms entering the Virial Theorem are derived, and the fiducial anisotropy limit required to prevent the onset of Radial Orbit Instability is determined as a function of the galaxy parameters. The presented models, built following an approach already adopted in our previous works, can be a useful starting point for a more advanced modeling of the dynamics of elliptical galaxies, and can be easily implemented in numerical simulations requiring a realistic dynamical model of a galaxy.

**Key words:** celestial mechanics – galaxies: kinematics and dynamics – galaxies: elliptical and lenticular, cD

## 1 INTRODUCTION

Spherically symmetric galaxy models, thanks to their simplicity, can be useful in exploratory works in Stellar Dynamics (e.g., Bertin 2000, Binney & Tremaine 2008). A successful spherical model compensates its geometric limitations with other features, such as the possibilities to derive manageable analytical expressions for the most important dynamical quantities, to easily include a dark matter (hereafter, DM) halo with an adjustable density profile (or, alternatively, to specify the total density profile), to model the dynamical effects of a central black hole (hereafter, BH), and finally to control orbital anisotropy. Once the model properties are controlled in the spherical limit, then more sophisticated investigations, based on axisymmetric or triaxial galaxy models, can be undertaken avoiding a large exploration of the parameter space (e.g., Cappellari et al. 2007, van den Bosch et al. 2008).

The analytical Jaffe (1983) density profile is a natural choice to describe the stellar distribution of early-type galaxies in the spherical approximation. It belongs to the family of the so-called  $\gamma$  models (Dehnen 1993, Tremaine et al. 1994), and resembles, in projection, the de Vaucouleurs law (1984)  $R^{1/4}$  with sufficient accuracy (for most applications) over a large radial range.

Once the stellar profile of the model is considered acceptable,

a second request is the possibility to reproduce, with a minor effort, the large scale properties of the *total* density profile (e.g. Bertin et al. 1994, Rix et al. 1997, Gerhard et al. 2001; Treu & Koopmans 2002, 2004; Rusin et al. 2003; Rusin & Kochanek 2005; Koopmans et al. 2006; Gavazzi et al. 2007; Czoske et al. 2008; Dye et al. 2008, Nipoti et al. 2008, see also Shankar et al. 2017). For example, simple models with a flat rotation curve have in fact been constructed (see, e.g., Kochanek 1994, Naab & Ostriker 2007, Ciotti et al. 2009, hereafter CMZ09; see also the double power-law models of Hiottelis 1994).

Finally, since supermassive BHs with a mass of the order of  $M_{\text{BH}} \simeq 10^{-3} M_*$  are routinely found at the center of the stellar spheroids of total mass  $M_*$  (e.g., see Magorrian et al. 1988, Kormendy & Ho 2013), another feature of a useful spherical model is the possibility to easily compute the dynamical properties of the stellar component in presence of a central BH.

Following the arguments above, a family of models (hereafter, JJ models) with a Jaffe profile for the stellar distribution, and a total density profile described by another Jaffe law, so that the total mass of JJ models kept finite, has already been proposed (Ciotti & Ziaee Lorzad 2018, hereafter CZ18). For the stellar component JJ models with a central BH, the Jeans equations with Osipkov–Merritt (Osipkov 1979, Merritt 1985, hereafter OM) radial anisotropy can

arXiv:1909.09639v1 [astro-ph.GA] 20 Sep 2019

be solved analytically, and the projected velocity dispersion, at the center and at large radii, can be expressed by means of simple formulae. Moreover, for these models also the positivity of the phase-space distribution function (hereafter, DF), the so-called consistency, and the maximum amount of radial anisotropy allowable for consistency, can be easily studied.

One interesting feature of the JJ models is that in the special *minimum halo* case, the DM profile, defined by the difference between the total and the stellar profiles, behaves like  $r^{-1}$  near the center, similarly to the Navarro-Frenk-White profile (Navarro et al. 1997, hereafter NFW); at large radii, instead, the DM profile decreases as  $r^{-4}$ , at variance with the NFW profile that goes as  $r^{-3}$ . The natural question left open is then if it is possible to construct models with similar analytical properties of JJ models, but with the additional property that the DM follows the  $r^{-3}$  shape in the external regions. In this paper we show that in fact this is possible, and we call the resulting models “J3”, to stress that the stellar density is again a Jaffe model, while the DM decreases as  $r^{-3}$  in the external regions. In particular, we shall prove that the DM halo, in minimum halo J3 models, can be made remarkably similar to the NFW over the *whole* radial range.

The paper is organized as follows. In Sect. 2 the main structural properties of the models are presented, and the conditions required to have a nowhere negative and monotonically decreasing DM halo density profile are derived; a discussion is also given of how the DM component can be built in order to have the same asymptotical behaviour, in the outer regions and near the center, as the NFW profile. In Sect. 3 we study the phase-space properties of the models, and the minimum value of the anisotropy radius for consistency is derived in terms of the galaxy parameters. In Sect. 4 the analytical solution of the Jeans equations with OM anisotropy is obtained, and the asymptotic trend of the projected velocity dispersion profile at small and large radii is given. Finally, in Sect. 5 the relevant global quantities entering the Virial Theorem are explicitly calculated; these are used for global energetic considerations, and to determine the fiducial anisotropy limit required to prevent the onset of Radial Orbit Instability as a function of the galaxy parameters. Section 6 summarizes.

## 2 THE MODELS

We name the proposed new family of models as “J3” models, to indicate two-component models characterized by a *stellar* density distribution  $\rho_*$  described by a Jaffe (1983) profile embedded in a *total* density distribution  $\rho_g$  (stars plus DM) following a  $r^{-2}$  profile in the central regions and  $r^{-3}$  at large radii. The reasons for this choice will become clear in the following.

### 2.1 Stellar distribution

As in CZ18, the stellar component follows a Jaffe profile, with density and relative potential scales given by

$$\rho_n \equiv \frac{M_*}{4\pi r_*^3}, \quad \Psi_n \equiv \frac{GM_*}{r_*}, \quad (1)$$

where  $M_*$  is the total stellar mass, and  $r_*$  a scale length. In these units, the stellar density-potential pair reads

$$\rho_*(r) = \frac{\rho_n}{s^2(1+s)^2}, \quad \Psi_*(r) = \Psi_n \ln \frac{1+s}{s}, \quad (2)$$

where  $s \equiv r/r_*$  is the dimensionless radius, and in general we indicate with  $\Psi(r) \equiv -\Phi(r)$  the relative potential. The cumulative

mass contained within the sphere of radius  $r$  is

$$M_*(r) = M_* \times \frac{s}{1+s}, \quad (3)$$

thus  $r_*$  is the half-mass (spatial) radius.

The projected density at radius  $R$  in the projection plane (see, e.g., Binney & Tremaine 2008) is written as

$$\Sigma_*(R) = 2 \int_R^\infty \frac{\rho_*(r)r}{\sqrt{r^2 - R^2}} dr = \frac{M_*}{r_*^2} \times f_*(\eta), \quad (4)$$

where  $\eta \equiv R/r_*$ , and  $f_*(\eta)$  is given in Appendix A. In particular,

$$\Sigma_*(R) \sim \frac{M_*}{r_*^2} \times \begin{cases} \frac{1}{4\eta}, & R \rightarrow 0, \\ \frac{1}{8\eta^3}, & R \rightarrow \infty. \end{cases} \quad (5)$$

Finally, the projected mass  $M_{p*}(R)$  contained within the cylinder of radius  $R$  is

$$M_{p*}(R) \equiv 2\pi \int_0^R \Sigma_*(R')R'dR' = M_* \times g_*(\eta), \quad (6)$$

where the function  $g_*(\eta)$  is given in Appendix A; as expected,  $g_*(\eta) \rightarrow 1$  for  $\eta \rightarrow \infty$ . In particular, by setting  $g_* = 1/2$  we obtain the well-known result that  $R_e \simeq 0.7447 r_*$ , where  $R_e$  is the effective radius of the Jaffe profile.

### 2.2 Total mass distribution

Following the considerations in the Introduction, the total (stars plus DM) mass density profile is

$$\rho_g(r) = \frac{\mathcal{R}\rho_n}{s^2(\xi+s)}, \quad \xi \equiv \frac{r_g}{r_*}, \quad (7)$$

where  $\mathcal{R}$  is a dimensionless factor, and  $r_g$  is the galaxy scale length. At variance with the stellar profile, the total mass is divergent, so that now  $\mathcal{R}$  cannot be defined as the ratio of the total-to-stellar mass (as in CZ18) but, more appropriately, as a *density* ratio. For example, from eqs. (2) and (7), it follows that  $\mathcal{R} = \xi\rho_g(r)/\rho_*(r)$  for  $r \rightarrow 0$ . In turn this means that the obvious request  $\rho_g(r) \geq \rho_*(r)$ , when considered for  $r \rightarrow 0$ , forces  $\mathcal{R} \geq \xi$ . In Section 2.3 we shall fully address the problem of the positivity of the DM density profile, obtained as the difference  $\rho_{DM}(r) = \rho_g(r) - \rho_*(r)$ , over the whole radial range.

The cumulative mass distribution associated with the total galaxy density is

$$M_g(r) = M_* \mathcal{R} \ln \frac{\xi+s}{\xi}, \quad (8)$$

and diverges logarithmically. Incidentally, eq. (8) allows for different interpretations of the parameter  $\mathcal{R}$ , in terms of cumulative masses inside some prescribed radius; for example,  $\mathcal{R} = M_g(r_g)/(M_* \ln 2)$ .

From a simple integration, the projected galaxy total density profile is

$$\Sigma_g(R) = \frac{M_*}{r_*^2} \frac{\mathcal{R}}{\xi^2} \times f_g(\eta), \quad (9)$$

where now  $\eta \equiv R/r_g$ , and  $f_g(\eta)$  is given in Appendix A, and

$$\Sigma_g(R) \sim \frac{M_* \mathcal{R}}{r_*^2 \xi^2} \times \begin{cases} \frac{1}{4\eta}, & R \rightarrow 0, \\ \frac{1}{2\pi\eta^2}, & R \rightarrow \infty. \end{cases} \quad (10)$$

The projected mass within a cylinder of radius  $R$  is

$$M_{\text{pg}}(R) = M_* \mathcal{R} \times g_{\text{g}}(\eta), \quad (11)$$

where the function  $g_{\text{g}}(\eta)$  is given in Appendix A, and  $g_{\text{g}}(\eta) \sim \ln \eta$  for  $\eta \rightarrow \infty$ . The gravitational potential can be easily determined; even though the total mass is infinite, yet the normalization value at infinity can still be assumed equal to zero, as the density profile at large radii is steeper than  $r^{-2}$ . The resulting relative potential associated with the density  $\rho_{\text{g}}(r)$  is

$$\Psi_{\text{g}}(r) = \Psi_{\text{n}} \mathcal{R} \times \left( \frac{1}{\xi} \ln \frac{\xi + s}{s} + \frac{1}{s} \ln \frac{\xi + s}{\xi} \right). \quad (12)$$

Note that the first term is nothing else than the rescaled Jaffe potential in eq. (2), and dominates in the central regions, while the second term becomes dominant at large radii.

As a BH of mass  $M_{\text{BH}} = \mu M_*$  is added at the center of the galaxy, the total mass profile is  $M_{\text{T}}(r) = M_{\text{g}}(r) + M_{\text{BH}}$ ; then the circular speed is given by

$$v_{\text{c}}^2(r) = \frac{\Psi_{\text{n}}}{s} \times \left( \mathcal{R} \ln \frac{\xi + s}{\xi} + \mu \right), \quad (13)$$

and in the very external regions the circular velocity falls to zero as

$$v_{\text{c}}^2(r) \sim \Psi_{\text{n}} \mathcal{R} \frac{\ln s}{s}. \quad (14)$$

### 2.3 The dark matter distribution: positivity and monotonicity

As already done for JJ models, we first study the conditions for the positivity and radial monotonicity of the DM halo density profile  $\rho_{\text{DM}}(r) = \rho_{\text{g}}(r) - \rho_*(r)$ . While the request of positivity for  $\rho_{\text{DM}}(r)$  is natural, we recall that monotonicity of the density is necessary for the positivity of the phase-space DF (Ciotti & Pellegrini 1992, hereafter CP92; see also Sect. 3).

Not all values of  $\mathcal{R}$  and  $\xi$  are compatible with a nowhere negative distribution

$$\rho_{\text{DM}}(r) = \frac{\rho_{\text{n}}}{s^2} \times \left[ \frac{\mathcal{R}}{\xi + s} - \frac{1}{(1 + s)^2} \right]. \quad (15)$$

Note that in general the DM-to-stellar mass ratio  $\rho_{\text{DM}}(r)/\rho_*(r)$  depends on  $r$ .

In Appendix B we determine the condition on  $\mathcal{R}$  and  $\xi$  such that  $\rho_{\text{DM}}(r) \geq 0$  for  $r \geq 0$ , obtaining

$$\mathcal{R} \geq \mathcal{R}_{\text{m}}(\xi) = \begin{cases} \frac{1}{4(1 - \xi)}, & 0 < \xi \leq \frac{1}{2}, \\ \xi, & \xi \geq \frac{1}{2}. \end{cases} \quad (16)$$

A DM halo of a model with  $\mathcal{R} = \mathcal{R}_{\text{m}}(\xi)$  is called a *minimum halo*. Notice that the condition in eq. (16) for  $\xi \geq 1/2$ , i.e.  $\mathcal{R} \geq \xi$  is coincident with that obtained in Sect. 2.2 from the preliminary analysis near the center; instead, for  $0 < \xi < 1/2$ , the condition is more stringent (see the dashed line in Fig. 1, left panel). This means that values of  $(\xi, \mathcal{R})$  between the dashed and solid lines in Fig. 1 correspond to  $\rho_{\text{DM}}(r)$  that becomes negative off-center. We stress that the formulae in the paper (if not differently stated) apply to  $\xi > 0$ , even if realistic cases (i.e., a total density profile shallower than the stellar one) are obtained for  $\xi \geq 1$ .

The positivity of  $\rho_{\text{DM}}(r)$  is just a first condition for the viability of the model. A second request, based on dynamical arguments (see Section 3.1), is the monotonicity of  $\rho_{\text{DM}}$  as a function of radius, and this reduces to the determination of the minimum value

$\mathcal{R}_{\text{mon}}$  so that  $d\rho_{\text{DM}}(r)/dr \leq 0$ . The explicit discussion is deferred to Appendix B, where we prove that, for  $\xi \geq 1/2$ , positivity and monotonicity of  $\rho_{\text{DM}}$  coincide (in analogy with what found for JJ models).

We discuss now the relative trend of DM and stars, both at large radii and near the center, as a function of  $\mathcal{R}$  and  $\xi$ . For  $r \rightarrow \infty$  it is easy to show that

$$\rho_{\text{DM}}(r) \sim \frac{\rho_{\text{n}} \mathcal{R}}{s^3}, \quad r \rightarrow \infty, \quad (17)$$

and so the DM is dominant over the stars. Close to the center, instead,

$$\rho_{\text{DM}}(r) = \frac{\rho_{\text{n}}}{\xi} \times \left( \frac{\mathcal{R} - \xi}{s^2} + \frac{2\xi^2 - \mathcal{R}}{\xi s} + \frac{\mathcal{R} - 3\xi^3}{\xi^2} + \dots \right), \quad (18)$$

so the trend depends on the values of  $\mathcal{R}$  and  $\xi$ . From eqs. (18) and (16) it follows that, in non-minimum halo models,  $\rho_{\text{DM}}(r) \propto r^{-2}$ , so the DM and stellar densities are locally proportional. In the minimum halo models we have  $\rho_{\text{DM}}(r) \propto r^{-2}$  for  $\xi < 1/2$ ,  $\rho_{\text{DM}}(r) \propto \text{constant}$  for  $\xi = 1/2$ , and finally  $\rho_{\text{DM}}(r) \propto r^{-1}$  for  $\xi > 1/2$ . In particular, in the latter case, when  $\mathcal{R} = \mathcal{R}_{\text{m}}(\xi) = \xi$ , one has

$$\rho_{\text{DM}}(r) \sim \rho_{\text{n}} \frac{2\xi - 1}{\xi s}, \quad r \rightarrow 0, \quad (19)$$

and so  $\rho_{\text{DM}}(r)$  is centrally shallower than  $\rho_*(r)$ . We shall discuss an interesting application of eqs. (17) and (19) at the end of this Section.

We evaluate now the relative amount of dark and visible mass within a prescribed spatial radius. The minimum value for this quantity is derived from eqs. (3) and (8) as

$$\frac{M_{\text{DM}}(r)}{M_*(r)} \geq \mathcal{R}_{\text{m}}(\xi) \frac{1 + s}{s} \ln \frac{\xi + s}{\xi} - 1, \quad (20)$$

where  $M_{\text{DM}}(r) = M_{\text{g}}(r) - M_*(r)$ . In Fig. 1 (middle panel) the mass ratios corresponding to three representative values of  $r$  are shown as a function of  $\xi$ . Note that, for fixed values of  $s$ , the function at the r.h.s. of eq. (20) tends to  $s$  for  $\xi \rightarrow \infty$ . A similar behavior is obtained for the ratio of the projected DM-to-visible mass within an aperture  $R$ ; from eqs. (6) and (11) one has

$$\frac{M_{\text{pDM}}(R)}{M_{\text{p}*}(R)} \geq \mathcal{R}_{\text{m}}(\xi) \frac{g_{\text{g}}(\eta/\xi)}{g_*(\eta)} - 1, \quad (21)$$

where  $\eta = R/r_*$ . In Fig. 1 (right panel), we plot this quantity as a function of  $\xi$  for three representative values of the aperture radius:  $R_{\text{e}}/2$ ,  $R_{\text{e}}$ , and  $2R_{\text{e}}$ . As for JJ models, the resulting functions of  $\xi$  are non monotonic.

We finally compare the DM halo profile in eq. (15) with the NFW profile (Navarro et al. 1997), which we rewrite as

$$\rho_{\text{NFW}}(r) = \frac{\rho_{\text{n}} \mathcal{R}_{\text{NFW}}}{f(c)s(\xi_{\text{NFW}} + s)^2}, \quad f(c) = \ln(1 + c) - \frac{c}{1 + c}, \quad (22)$$

where for a chosen radius  $r_{\text{t}}$ , we define  $\mathcal{R}_{\text{NFW}} \equiv M_{\text{NFW}}(r_{\text{t}})/M_*$ ,  $\xi_{\text{NFW}} \equiv r_{\text{NFW}}/r_*$  is the NFW scale length in units of  $r_*$ , and  $c \equiv r_{\text{t}}/r_{\text{NFW}}$ . By construction,  $\rho_{\text{DM}}(r)$  and  $\rho_{\text{NFW}}(r)$  at large radii have the same behaviour. Moreover, at small radii, where  $\rho_{\text{NFW}}(r) \propto r^{-1}$ , in the minimum halo case with  $\xi > 1/2$ , one also has that  $\rho_{\text{DM}}(r) \propto r^{-1}$ . Remarkably, from eqs. (17) and (19) it follows that  $\rho_{\text{DM}}(r)$  and  $\rho_{\text{NFW}}(r)$  can be made asymptotically *identical* in the outer regions and near the center, just by imposing

$$\frac{\mathcal{R}_{\text{NFW}}}{f(c)} = \xi, \quad \xi_{\text{NFW}} = \frac{\xi}{\sqrt{2\xi - 1}}. \quad (23)$$

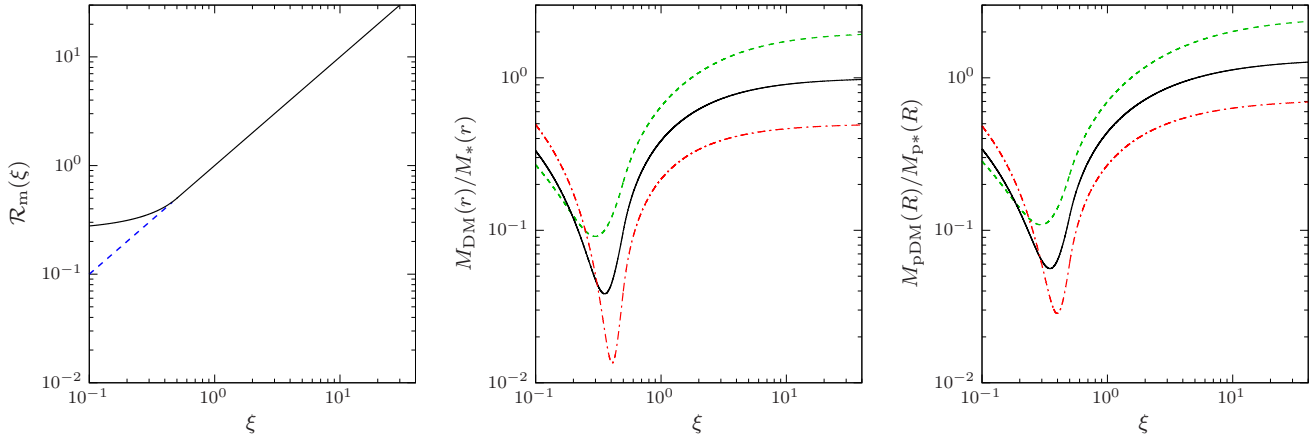


**Figure 1.** Left panel: the function  $\mathcal{R}_m(\xi)$ , as given by eq. (16). Only models in the region above the black solid line have a DM halo with a nowhere negative  $\rho_{\text{DM}}(r)$ . Central panel: the minimum value of the volumic DM-to-stellar mass ratio, given in eq. (20), inside a sphere of radius  $r = 0.5r_*, r_*, 2r_*$  (red dash-dotted, black solid and green dashed lines, respectively), as a function of  $\xi$ . Right panel: the minimum value of the projected DM-to-stellar mass ratio, given in eq. (21), inside the circle of radius  $R = 0.5R_e, R_e, 2R_e$  (red dash-dotted, black solid and green dashed lines, respectively), as a function of  $\xi$ . See Sect. 2.3 for more details.

Therefore, once a specific minimum halo galaxy model with  $\xi \geq 1/2$  is considered, and then  $\rho_n$  and  $\xi$  are chosen, eqs. (22) and (23) allow to determine the NFW profile that best reproduces  $\rho_{\text{DM}}(r)$  by tuning the value of the ratio  $\mathcal{R}_{\text{NFW}}/f(c)$ . As pointed out in the Introduction, the possibility to have a DM distribution very similar to the NFW profile both at the center *and* in the outer regions makes J3 models an improvement over JJ models, whose DM profile is necessarily more and more discrepant from the NFW profile with increasing radii.

Figure 2 (left panel) shows an example of how well a NFW profile can reproduce a minimum halo  $\rho_{\text{DM}}(r)$ , when both profiles are chosen in a cosmologically motivated way. In this figure  $\xi = 13$  and  $c = 10$ , that give, from eq. (23),  $\mathcal{R}_{\text{NFW}} \simeq 20$ , as expected on the scale of massive galaxies from cosmological simulations and galaxy-halo abundance matching technique (e.g., Bullock & Boylan-Kolchin 2017). For this model  $r_{\text{NFW}} = 2.6 r_*$  from eq. (23), and the right panel in Fig. 2 shows the different contributions of the various mass component to the circular velocity  $v_c(r)$ .

### 3 THE PHASE-SPACE DISTRIBUTION FUNCTION

We now proceed to recover the OM phase-space DF for J3 models in presence of a central BH. Indeed, for OM models it is possible to obtain lower bounds for the anisotropy radius without actually recovering the DF (that only exceptionally can be expressed in terms of elementary or known functions; see, e.g., CP92, Ciotti 1996, Ciotti 1999). We shall use, as for JJ models, a result presented in CP92<sup>1</sup>.

We therefore consider, for the stellar component, a DF of the family

$$f = f(Q), \quad Q \equiv \mathcal{E} - \frac{J^2}{2r_a^2}, \quad (24)$$

<sup>1</sup> The conditions in CP92 are a special case of a more general family of inequalities (see, e.g., de Bruijne et al. 1996, An & Evans 2006, Ciotti & Morganti 2009, 2010ab, van Hese et al. 2011, and references therein).

(e.g., Binney & Tremaine 2008), where  $r_a$  is the anisotropy radius, and  $\mathcal{E} = \Psi_{\text{T}} - v^2/2$  and  $J$  are the relative energy and angular momentum modulus of each star (per unit mass); moreover,  $f(Q) = 0$  for  $Q < 0$ . The total (relative) gravitational potential is  $\Psi_{\text{T}}(r) = \Psi_{\text{g}}(r) + GM_{\text{BH}}/r$ , and from eq. (12) one has

$$\frac{\Psi_{\text{T}}(r)}{\Psi_n} \equiv \psi(r) = \mathcal{R} \left( \frac{1}{\xi} \ln \frac{\xi + s}{s} + \frac{1}{s} \ln \frac{\xi + s}{\xi} \right) + \frac{\mu}{s}. \quad (25)$$

The anisotropy profile is given by

$$\beta(r) \equiv 1 - \frac{\sigma_t^2(r)}{2\sigma_r^2(r)} = \frac{r^2}{r^2 + r_a^2}, \quad (26)$$

where  $\sigma_r(r)$  and  $\sigma_t(r)$  are the radial and tangential components of the velocity dispersion tensor, respectively. The fully isotropic case is obtained for  $r_a \rightarrow \infty$ , while for  $r_a = 0$  the galaxy is supported by radial orbits only. For finite values of  $r_a$ , instead, the velocity dispersion tensor becomes isotropic for  $r \rightarrow 0$ , and fully radially anisotropic for  $r \rightarrow \infty$ .

The phase-space DF of the stellar component reads

$$f(Q) = \frac{1}{\sqrt{8\pi^2}} \int_0^Q \frac{d^2\varrho}{d\Psi_{\text{T}}^2} \frac{d\Psi_{\text{T}}}{\sqrt{Q - \Psi_{\text{T}}}}, \quad (27)$$

where

$$\varrho(r) \equiv \rho_*(r) \times \left( 1 + \frac{r^2}{r_a^2} \right) \quad (28)$$

is intended expressed in terms of  $\Psi_{\text{T}}$  by elimination of radius.

#### 3.1 Necessary and sufficient conditions for consistency

Before the numerical reconstruction of the DF and the determination of the critical value of  $r_a$  for consistency, it is instructive to study preliminarily the limitations on the anisotropy radius obtained by the request of  $f(Q) \geq 0$  over the accessible phase-space. The CP92 *necessary condition* for the positivity of the DF of each mass component of J3 models in the total potential is that

$$\frac{d\varrho(r)}{dr} \leq 0, \quad [\text{NC}]. \quad (29)$$

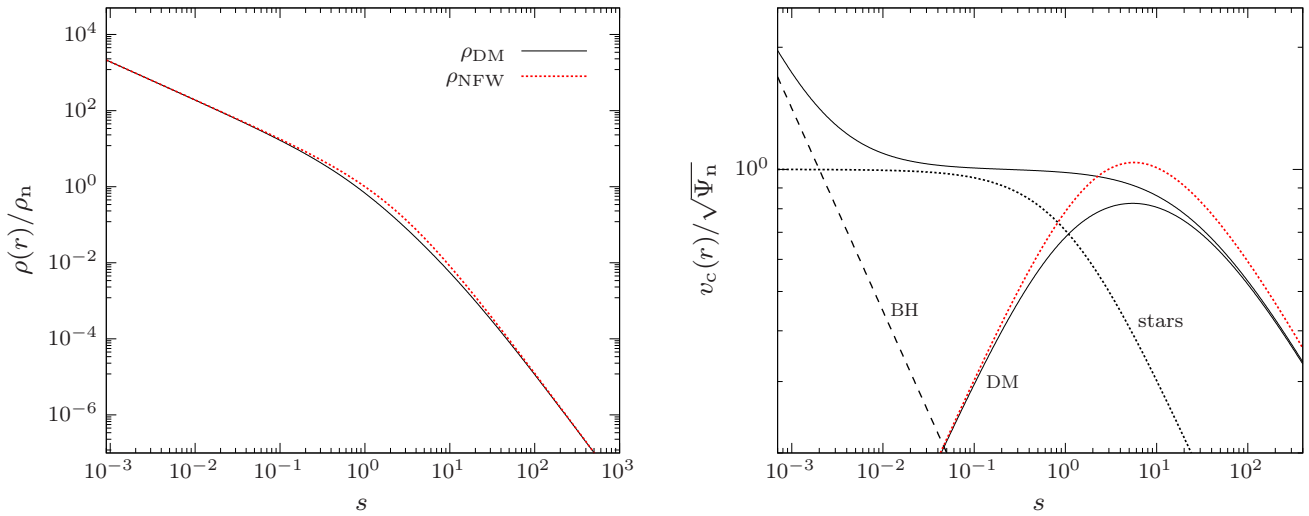


**Figure 2.** Left panel: comparison between the minimum halo DM profile of J3 models (black solid line) and the NFW profile (red dotted line), for  $\xi = 13$  and  $c = 10$ . Right panel: circular velocity profile for the same minimum halo galaxy model with  $\mu = 0.002$  (solid line), with the separate contributions of BH, stars and the DM halo for the J3 model; the circular velocity profile associated with the density  $\rho_{NFW}(r)$  in the left panel (red dotted line) is also shown. See Sect. 2.3 for more details.

Notice how this condition is actually independent of the presence of other density components. Moreover, a *weak sufficient condition* for consistency reads

$$\frac{d}{dr} \left[ \frac{d\varrho(r)}{dr} \frac{r^2}{M_T(r)} \right] \geq 0, \quad [\text{WSC}], \quad (30)$$

where it is apparent that, at variance with the NC, the WSC depends also on the radial density profile of the other components. Summarizing, a model failing eq. (29) is certainly inconsistent, while a model obeying eq. (30) is certainly consistent. Hence, the limitations obtained from the applications of the two previous inequalities are expected to “bracket” the true limitations on the model parameters, which can be only determined by direct inspection of the DF.

Before embarking on the analysis of the consistency, we recall a couple of points. The first concerns the effect of the central BH on consistency. From eq. (30) it follows that if 1) the investigated density component satisfies the WSC for  $M_{BH} = 0$ , and 2)  $d(r^2 d\varrho/dr)/dr \geq 0$ , then the WSC is satisfied<sup>2</sup> for arbitrary values of  $M_{BH}$ . The second consideration is about the effect of orbital anisotropy. In fact, the investigation of the NC and WSC, and the study of the DF positivity in eq. (27), all lead to consider inequalities that can be written as

$$F + \frac{G}{s_a^2} \geq 0, \quad s_a \equiv \frac{r_a}{r_*}, \quad (31)$$

and that must hold over the domain  $\mathcal{C}$  spanned by the arguments of the functions  $F$  and  $G$ . For example, in case of the DF these two functions are given by eq. (34), with argument  $q$ ; or, in case of NC and WSC, by the radial functions obtained from eq. (28). In the following we discuss the DF case. Equation (31) shows that all OM models can be divided in two families. In the first case, when  $F$  is nowhere negative over  $\mathcal{C}$  (e.g., in the case of a consistent isotropic

DF), consistency is obtained for

$$s_a \geq s_a^- \equiv \sqrt{\max \left[ 0, \sup_{\mathcal{C}} \left( -\frac{G}{F} \right) \right]}. \quad (32)$$

If  $G \geq 0$ , then  $s_a^- = 0$  and the system can be supported by radial orbits only. In the second case,  $F \geq 0$  over some subset  $\mathcal{C}_+$  of  $\mathcal{C}$ , and negative (or zero) over the complementary subset  $\mathcal{C}_-$ . If also  $G < 0$  somewhere on  $\mathcal{C}_-$ , then the model is inconsistent. If  $G \geq 0$  on  $\mathcal{C}_-$  one must consider the lower limit  $s_a^-$  evaluated over  $\mathcal{C}_+$  as above, *and* the upper limit

$$s_a \leq s_a^+ = \sqrt{\inf_{\mathcal{C}_-} \left( -\frac{G}{F} \right)}, \quad (33)$$

over  $\mathcal{C}_-$ : consistency is possible only if  $s_a^- < s_a^+$ .

The first application of the NC and WSC to J3 models concerns the consistency of the DM halo. For simplicity, we restrict to the isotropic case, when eq. (29) shows the equivalence of the NC with the request of monotonicity of  $\rho_{DM}(r)$ : remarkably, according to the results in eqs. (B2)-(B3), for  $\xi \geq 1/2$  the NC is satisfied once just positivity is assured, i.e. for  $\mathcal{R} \geq \xi$ . The WSC for the isotropic DM halo with a central BH requires in general a numerical study: following the considerations after eq. (30), in Appendix B we prove that for  $\xi \geq 1$  the WSC is satisfied once  $\mathcal{R} \geq \xi$ . This means that for isotropic DM halos of J3 models with a central BH and  $\xi \geq 1$ , the requirements of positivity, monotonicity, and WSC for phase-space consistency coincide, and are all satisfied once  $\mathcal{R} \geq \xi$ .

We now apply the NC and WSC to the Jaffe stellar component of J3 models. We recall that the NC of a pure Jaffe model just reduces to  $s_a \geq 0$ , while the WSC gives  $s_a \geq s_a^- \simeq 0.1068$  (e.g., Ciotti 1999, CZ18). In Appendix B we show that the WSC always produces the case described by eq. (32), i.e. only  $s_a^-$  exists. When restricting to the case  $\mu = 0$  the limit on anisotropy is independent of  $\mathcal{R}$ , and by numerical solution of eq. (B5) we obtain  $s_a^- = s_a^-(\xi)$  (dotted red line in Fig. 3). At the opposite limit we have the BH dominated case (see Appendix A of CZ18), with  $s_a^- \simeq 0.31$ , obviously independent of  $\xi$  and  $\mu$ . Again following the discussion after

<sup>2</sup> The conditions 1) and 2) are special cases of a more general result of easy proof, i.e., the fact that eq. (30) is necessarily true once it is separately true for  $\varrho(r)$  in each mass component producing  $M_T(r)$ .

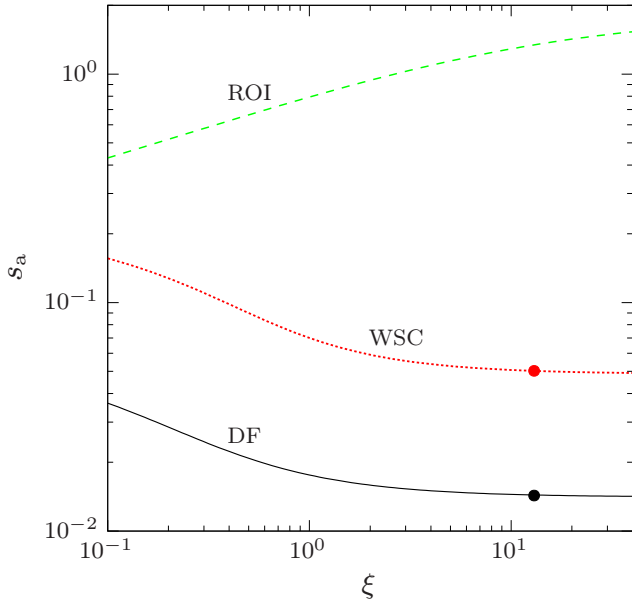


**Figure 3.** Different limitations on the anisotropy radius  $s_a = r_a/r_*$  of the stellar component of J3 models, as a function of  $\xi = r_g/r_*$ . The lines refer to  $\mu = 0$ , i.e. in absence of the central BH. The black solid line and the red dotted line represent the minimum value of  $s_a$  obtained directly from the DF and from the WSC (see eq. [B5]), respectively, while the green dashed curve represents the fiducial lower limit of  $s_a$  to prevent the onset of Radial Orbit Instability (see Sect. 5.1). The circles correspond to models with  $\xi = 13$ , for which we find  $s_a^- \simeq 0.0143$  (DF) and  $s_a^- \simeq 0.0502$  (WSC). For reference, the minimum value for consistency for the Jaffe model is  $s_a^- \simeq 0.02205$ .

eq. (30), from comparison with Fig. 3 we conclude that the stellar component of J3 models is certainly consistent for  $s_a \geq 0.31$ .

Summarizing, for J3 models this preliminary analysis reveals that the presence of a diffuse halo allows for the possibility of more radial orbits, while a concentrated halo requires a more isotropic velocity dispersion tensor for stellar consistency (for similar results see, e.g., Ciotti 1996, 1999; CMZ09; CZ18).

### 3.2 Explicit phase-space DF

With the introduction of the dimensionless potential  $\psi = \Psi_T/\Psi_n$ , and the normalized augmented density  $\tilde{\varrho} = \varrho/\rho_n$ , eq. (27) becomes

$$\begin{aligned} f(q) &= \frac{\rho_n}{\sqrt{8}\pi^2\Psi_n^{3/2}} \int_0^q \frac{d^2\tilde{\varrho}}{d\psi^2} \frac{d\psi}{\sqrt{q-\psi}} \\ &= \frac{\rho_n}{\sqrt{8}\pi^2\Psi_n^{3/2}} \left[ U(q) + \frac{V(q)}{s_a^2} \right], \end{aligned} \quad (34)$$

where  $q \equiv Q/\Psi_n$ , and, from eq. (25),  $0 \leq q \leq \infty$ . Note how the resulting expression belongs to the family in eq. (31).

In the case of a pure stellar Jaffe model the functions  $U(q)$  and  $V(q)$  can be obtained analytically, as also for a Jaffe model with a central dominant BH; moreover, the function  $\tilde{\varrho}(\psi)$  for JJ models with a central BH can be obtained analytically (e.g., see Appendix C of CZ18, and references therein). Unfortunately, for J3 models  $U(q)$  and  $V(q)$  cannot be obtained in terms of elementary functions. Therefore, in the following discussion we shall proceed with the numerical integration of eq. (34) for a selected choice of the model parameters, changing the integration variable from potential

to radius, so that the integrand can be written as an explicit analytical function.

First, we determine numerically the lower limit on  $s_a$  for consistency by inspection of the functions  $U(q)$  and  $V(q)$ . Note that in absence of the central BH ( $\mu = 0$ ), from eq. (25) the variable  $q$  can be further scaled as  $\tilde{q} = q/\mathcal{R}$ , and the quantity  $\mathcal{R}^{-3/2}$  can be explicitly factored out in the functions  $U(q)$  and  $V(q)$  (see also eq. [C4] in CZ18). In particular, for models without a central BH, the position of the maximum in eq. (32) depends on  $\tilde{q}$ , and the value of  $s_a^-$  is independent of  $\mathcal{R}$ . It is numerically found that  $U(q) \geq 0$ , so that eq. (32) applies and only  $s_a^-$  exists: the black solid line in Fig. 3 shows the corresponding  $s_a^-(\xi)$ . At fixed  $\xi$ , anisotropy values  $s_a \geq s_a^-$  correspond to a positive DF. Notice how the shape of the critical consistency curve parallels the WSC condition (red dotted line). For reference, the black circle at  $\xi = 13$  marks the minimum anisotropy radius ( $s_a^- \simeq 0.0143$ ) for our representative J3 model. From Fig. 3 it is also apparent how the effect of a concentrated DM halo reduces the ability of the stellar component to sustain radial orbits, a common property of the OM models, confirming the trend obtained from the WSC. Here we mention a point of little practical interest, but quite relevant conceptually. Indeed, in CZ18 was shown that for the single component Jaffe model the OM DF requires, for consistency,  $s_a^- \simeq 0.02205$ , and so one could argue that the purely radial Jaffe model does not exist. However, the analytical DF for this particular model is positive, thus showing that the purely radial case is a singular limit for the OM DF: indeed, eqs. (C8) and (C10) in CZ18 show that the Jaffe stellar component of J3 models can be supported by radial orbits only. In any case this situation has not practical interest, as illustrated in Sect. 5.1.

Figure 4 shows the numerically recovered DF of the stellar component of a selection of J3 models, namely the minimum halo models with  $\mathcal{R} = \xi = 10$  (black lines) and  $\mathcal{R} = \xi = 20$  (red lines), in the isotropic (top panel) and anisotropic (bottom panel,  $s_a = 0.02$ ) cases; the DFs are shown with and without the effect of the central BH. For illustration, also the BH dominated DF (green dashed line) is shown. It is clear how at high relative energies the DF of the J3 models with a central BH is matched by the BH dominated DF, and how the values of the isotropic and anisotropic DFs become coincident. As in JJ models, the DFs with the central BH are lower at high relative energies than in the analogous models without the central BH, the same happens at low relative energies for models with heavier and extended halos. These can be qualitatively interpreted when considering that the DF values are expected to be inversely proportional to the cube of velocity dispersion, so that high velocity dispersions are expected to correspond to low values of the DF (cfr. with Fig. 5). We also notice that the curves relative to DFs in the strongly anisotropic cases behave (qualitatively) as the DFs of other OM models discussed in Ciotti & Lanzoni 1997 (Fig. 2), Ciotti 1999 (Figs. 2 and 3), CMZ09 (Fig. 3), and CZ18 (Fig. 3). In practice, in OM models small values of  $s_a$  lead to a depression of the DF at intermediate energies, where model inconsistency finally sets in when  $s_a$  drops below the consistency limit.

## 4 JEANS EQUATIONS WITH OM ANISOTROPY

The Jeans equations for spherical systems with general anisotropy has been discussed in Binney & Mamon (1982), and in the OM models the formal solution can be written as

$$\rho_*(r)\sigma_r^2(r) = \frac{G}{r^2 + r_a^2} \int_r^\infty \rho_*(x)M_T(x) \left(1 + \frac{r_a^2}{x^2}\right) dx$$

$$= \rho_n \Psi_n \frac{\mathcal{A}(s) + s_a^2 \mathcal{I}(s)}{s^2 + s_a^2}, \quad (35)$$

where in our case

$$\mathcal{I}(s) = \mathcal{R} \mathcal{I}_g(s) + \mu \mathcal{I}_{\text{BH}}(s), \quad (36)$$

$$\mathcal{A}(s) = \mathcal{R} \mathcal{A}_g(s) + \mu \mathcal{A}_{\text{BH}}(s). \quad (37)$$

In the two radial functions above the parameters  $\mathcal{R}$  and  $\mu$  have been explicitly factorized; for  $s_a \rightarrow \infty$  the solution of the fully isotropic case is recovered, while for  $s_a = 0$  one reduces to the purely radial case.

#### 4.1 The velocity dispersion profile

The BH contribution to the velocity dispersion profile is given by

$$\mathcal{I}_{\text{BH}}(s) = \frac{12s^3 + 6s^2 - 2s + 1}{3s^3(1+s)} + 4 \ln \frac{s}{1+s}, \quad (38)$$

$$\mathcal{A}_{\text{BH}}(s) = \frac{1+2s}{s(1+s)} + 2 \ln \frac{s}{1+s}. \quad (39)$$

The galaxy contribution is obtained with an integration by parts, and it can be written as

$$\mathcal{I}_g(s) = \mathcal{I}_{\text{BH}}(s) \ln \frac{\xi + s}{\xi} + \mathcal{F}_{\text{iso}}(\xi, s), \quad (40)$$

$$\mathcal{A}_g(s) = \mathcal{A}_{\text{BH}}(s) \ln \frac{\xi + s}{\xi} + \mathcal{F}_{\text{rad}}(\xi, s), \quad (41)$$

in which

$$\mathcal{F}_{\text{iso}}(\xi, s) \equiv \begin{cases} \frac{9\xi^2 + 3\xi + 1}{3\xi^3} \ln \frac{\xi + s}{s} + \frac{1}{\xi - 1} \ln \frac{\xi + s}{1+s} + \\ - \frac{2(1+3\xi)s - \xi}{6\xi^2 s^2} - 4\mathcal{H}(\xi, s), \\ \frac{13}{3} \ln \frac{1+s}{s} - \frac{2s^2 + 7s - 1}{6s^2(1+s)} - 4\mathcal{H}(1, s), \end{cases} \quad (42)$$

$$\mathcal{F}_{\text{rad}}(\xi, s) \equiv \begin{cases} \frac{1}{\xi} \ln \frac{\xi + s}{s} + \frac{1}{\xi - 1} \ln \frac{\xi + s}{1+s} - 2\mathcal{H}(\xi, s), \\ \ln \frac{1+s}{s} + \frac{1}{1+s} - 2\mathcal{H}(1, s), \end{cases} \quad (43)$$

where in eqs. (42) and (43) the first formula holds for  $\xi \neq 1$ , and the second for  $\xi = 1$ ; the function  $\mathcal{H}(\xi, s)$  is given in Appendix C.

An insight into the behavior of  $\sigma_r(r)$  is given by the expansion for  $r \rightarrow \infty$  and  $r \rightarrow 0$  of the obtained formulae. We begin with the outer galaxy regions, where

$$\mathcal{I}_{\text{BH}}(s) = \frac{1}{5s^5} + \mathcal{O}\left(\frac{1}{s^6}\right), \quad \mathcal{A}_{\text{BH}}(s) = \frac{1}{3s^3} + \mathcal{O}\left(\frac{1}{s^4}\right), \quad (44)$$

and, from expansion of eq. (C1), we obtain

$$\mathcal{I}_g(s) = \frac{\ln s}{5s^5} + \frac{1-5 \ln \xi}{25s^5} + \mathcal{O}\left(\frac{\ln s}{s^6}\right), \quad (45)$$

$$\mathcal{A}_g(s) = \frac{\ln s}{3s^3} + \frac{1-3 \ln \xi}{9s^3} + \mathcal{O}\left(\frac{\ln s}{s^4}\right). \quad (46)$$

From eqs. (35), (45) and (46), it follows that at large radii

$$\sigma_r^2(r) \sim \frac{\Psi_n \mathcal{R} \ln s}{s} \times \begin{cases} \frac{1}{5}, & s_a = \infty, \\ \frac{1}{3}, & s_a < \infty. \end{cases} \quad (47)$$

Therefore, at the lowest order,  $\sigma_r(r)$  in the outer regions is independent of  $\xi$ , and the asymptotic formula is similar to that of J3 models (which just differs in the absence of the function  $\ln s$ ).

The other important region for observational and theoretical works is the galaxy center: here the velocity dispersion profile is dominated by the BH contribution, with

$$\mathcal{I}_{\text{BH}}(s) = \frac{1}{3s^3} + \mathcal{O}\left(\frac{1}{s^2}\right), \quad \mathcal{A}_{\text{BH}}(s) = \frac{1}{s} + \mathcal{O}(\ln s), \quad (48)$$

while

$$\mathcal{I}_g(s) = \frac{1}{2\xi s^2} + \mathcal{O}\left(\frac{1}{s}\right), \quad \mathcal{A}_g(s) = -\frac{\ln s}{\xi} + \mathcal{O}(1). \quad (49)$$

Hence, as  $r \rightarrow 0$ ,

$$\sigma_r^2(r) \sim \frac{\Psi_n \mu}{s} \times \begin{cases} \frac{1}{3}, & s_a > 0, \\ 1, & s_a = 0. \end{cases} \quad (50)$$

If the central BH is absent, instead, one has

$$\sigma_r^2(r) \sim \frac{\Psi_n \mathcal{R}}{\xi} \times \begin{cases} \frac{1}{2}, & s_a > 0, \\ -\ln s, & s_a = 0, \end{cases} \quad (51)$$

and so, with the exception of the purely radial case,

$$\sigma_r^2(0) = \frac{\Psi_n \mathcal{R}}{2\xi}. \quad (52)$$

We notice that as a check of the obtained asymptotic formulae, we also expanded the integral in eq. (35) in the relevant regimes, recovering eqs. (45)-(46) and eqs. (48)-(49).

The properties of  $\sigma_r(r)$  are illustrated in Fig. 5 (top panel) for the representative J3 models with  $\mathcal{R} = \xi = 13$ . In particular, the effects of the central BH, of the DM halo, and of orbital anisotropy can be clearly seen at large radii, where the radially anisotropic  $\sigma_r(r)$  (red lines) are above those in the corresponding isotropic cases, a well known consequence of the OM parametrization. Note also how the isotropic and anisotropic profiles coincide in the central regions, in accordance with the analytical results in eqs. (50) and (51).

#### 4.2 Projected velocity dispersion

The projected velocity dispersion profile associated with a general anisotropy function  $\beta(r)$  is given by

$$\Sigma_*(R) \sigma_p^2(R) = 2 \int_R^\infty \left[ 1 - \beta(r) \frac{R^2}{r^2} \right] \frac{\rho_*(r) \sigma_r^2(r) r dr}{\sqrt{r^2 - R^2}}, \quad (53)$$

(e.g., Binney & Tremaine 2008), where, in the case of OM anisotropy,  $\beta(r)$  is defined in eq. (26).

Unsurprisingly the projection integral cannot be evaluated analytically for J3 models in terms of elementary functions. However, using eq. (35), and changing the order of integration, we find that, for a general OM model, eq. (53) can be rewritten as

$$\Sigma_*(R) \sigma_p^2(R) = G \int_R^\infty \mathcal{X}(r, R) \rho_*(r) M_T(r) \left( 1 + \frac{r_a^2}{r^2} \right) dr, \quad (54)$$

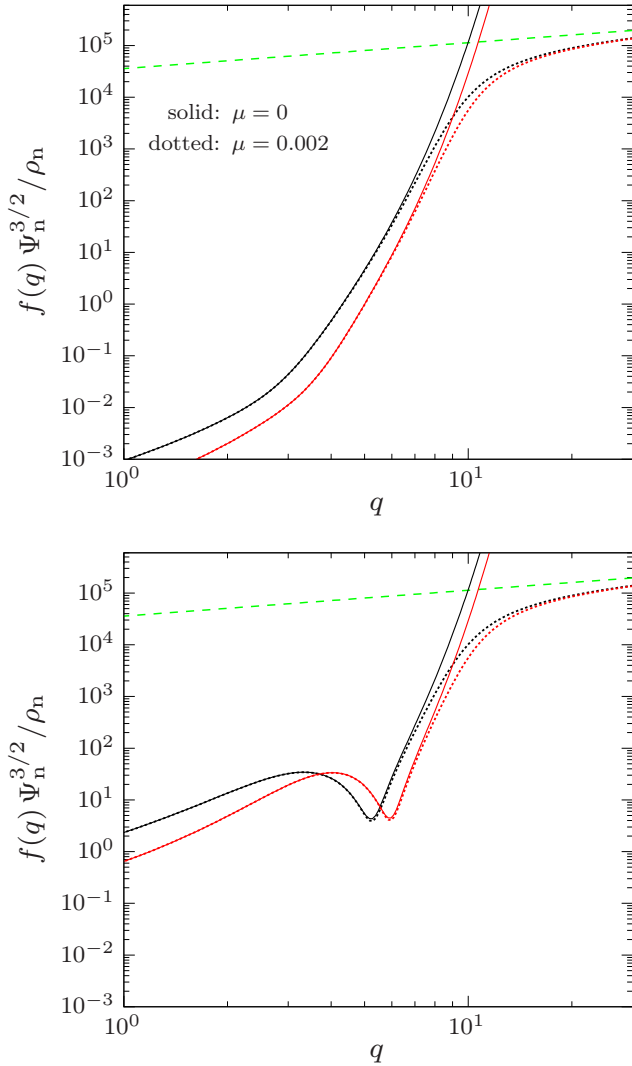


**Figure 4.** The DF of the stellar component for a minimum halo galaxy model with  $\mathcal{R} = \xi = 10$  (black lines) and  $\mathcal{R} = \xi = 20$  (red lines), in the isotropic (top panel) and anisotropic (bottom panel,  $s_a = 0.02$ ) cases. The DFs are shown with and without (dotted and solid lines, respectively) the effect of the central BH (with  $\mu = 0.002$ ). The green dashed line shows the DF of the Jaffe model in the BH dominated case (see Sect. 3.2).

where

$$\mathcal{K}(r, R) = \frac{2r_a^2 + R^2}{(r_a^2 + R^2)^{3/2}} \arctg \sqrt{\frac{r^2 - R^2}{r_a^2 + R^2}} - \frac{R^2 \sqrt{r^2 - R^2}}{(r_a^2 + R^2)(r_a^2 + r^2)}. \quad (55)$$

The special case  $r_a = 0$  and  $R = 0$  can be treated directly in eq. (53). Equations (54)-(55), although seem rather complicated, actually reduce the dimensionality of the integral (53) from two to one. This is an useful property in numerical works, avoiding the task of the computation of the two-dimensional integral (53). All the relevant properties of  $\sigma_p(R)$  are illustrated in the bottom panel of Fig. 5. As expected, in the outer regions the radially anisotropic profiles are below those in the corresponding isotropic cases, a natural result due to the projection effect on the radial orbit population. More quantitatively, the behaviour of  $\sigma_p(R)$  at large radii can be described by considering the leading term of the asymptotic expansion of the integral in eq. (53) for  $R \rightarrow \infty$ . There are no math-

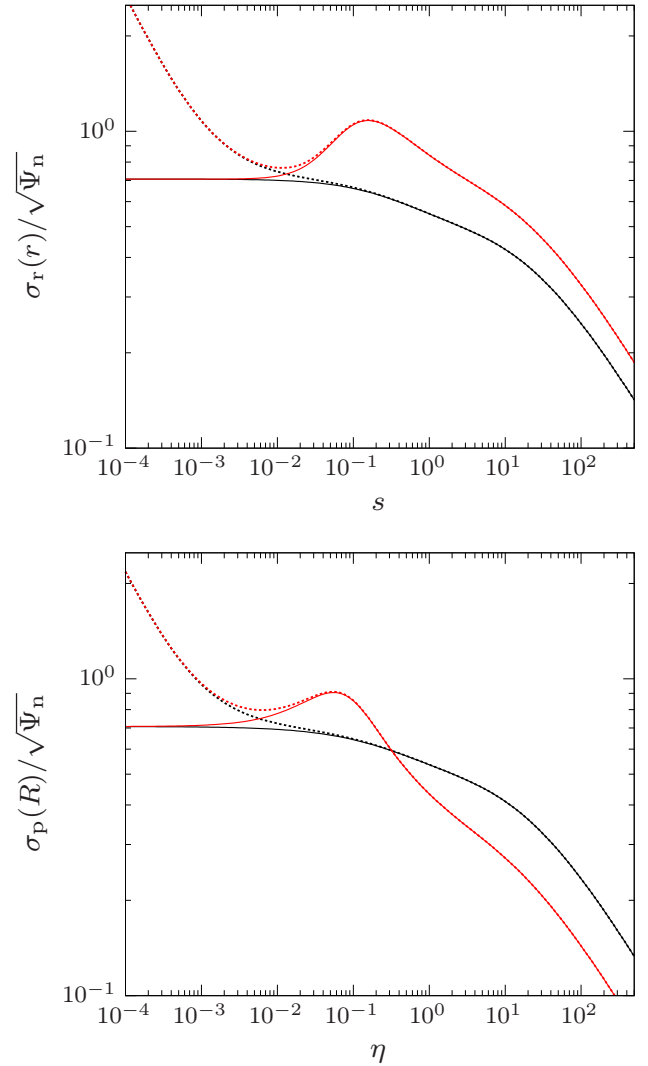


**Figure 5.** Top panel: radial trend of  $\sigma_r$  of the stellar component for a minimum halo model with  $\mathcal{R} = \xi = 13$ . Black lines refer to the isotropic case, red lines show the quite anisotropic case with  $s_a = 0.1$ . Bottom panel: radial trend of the projected stellar velocity dispersion  $\sigma_p$  versus  $\eta = R/r_*$  for the same model in the top panel. In both panels, the radial trends are shown with and without (dotted and solid lines, respectively) the effect of the central BH (with  $\mu = 0.002$ ).

ematical difficulties; the only care required is to take into account the effect of the radial anisotropy, and to distinguish two different cases, i.e., the isotropic case and any other model with finite  $s_a$ . We obtain:

$$\sigma_p^2(R) \sim \frac{8\Psi_n \mathcal{R} \ln \eta}{15\pi\eta} \times \begin{cases} 1, & s_a = \infty, \\ \frac{1}{3}, & s_a < \infty, \end{cases} \quad (56)$$

where  $\eta \equiv R/r_*$ . Notice the similarity of this result with that obtained for JJ models (see eq. [53] of CZ18). The numerical coefficients are identical, but now there is an additional logarithmic factor, and the BH mass ( $\mu$ ) does not appear because the total mass is infinite. Of course, also the coefficient  $\mathcal{R}$  is not the same quantity as in JJ models.

In the central regions both the integral in eq. (53) and  $\Sigma_*(R)$  diverge, so that  $\sigma_p(R)$  can be properly defined only as a limit. For

what concerns the *galaxy* contribution we have

$$\sigma_p(0) = \sigma_r(0), \quad s_a > 0, \quad (57)$$

where  $\sigma_r(0)$  is given by eq. (52). For  $r_a = 0$ , instead,  $\sigma_p^2(R) \sim -\sigma_r^2(0) \ln \eta$ . In presence of the central BH,  $\sigma_r(r)$  and  $\sigma_p(R)$  are dominated by the BH contribution, and from eqs. (50) and (53) we obtain

$$\sigma_p^2(R) \sim \frac{2\Psi_n \mu}{3\pi\eta}, \quad s_a \geq 0. \quad (58)$$

The independence of  $\sigma_p(R)$  from the specific value of  $s_a$  in the central regions is shown in the bottom panel of Fig. 5. Note that eqs. (57) and (58) coincide with their analogues for JJ models.

## 5 VIRIAL, POTENTIAL, AND KINETIC ENERGIES

Among the several global quantities associated with a stellar system, those entering the Virial Theorem (hereafter, VT) are certainly the most interesting for many observational and theoretical studies (e.g., Ciotti 2000, Binney & Tremaine 2008). For the stellar component of J3 models we have

$$2K_* = -W_* \equiv -(W_{*g} + W_{*BH}), \quad (59)$$

where

$$K_* = 2\pi \int_0^\infty \rho_*(r) [\sigma_r^2(r) + \sigma_t^2(r)] r^2 dr \equiv K_{*g} + K_{*BH} \quad (60)$$

is the total kinetic energy of the stars,

$$W_{*g} = -4\pi G \int_0^\infty \rho_*(r) M_g(r) r dr \quad (61)$$

is the interaction energy of the stars with the gravitational field of the galaxy (stars plus DM), and finally

$$W_{*BH} = -4\pi G M_{BH} \int_0^\infty \rho_*(r) r dr \quad (62)$$

is the interaction energy of the stars with the central BH. For a Jaffe galaxy  $W_{*BH}$  diverges; the VT implies that also  $K_{*BH}$  diverges.

The contribution of the total galaxy potential to  $W_{*g} = W_{**} + W_{*DM}$  (where  $W_{**}$  is due to the self-interaction of the stellar distribution, and  $W_{*DM}$  to the effect of the DM halo) is finite, and  $W_{*g}$  is written as

$$W_{*g} = -\Psi_n M_* \mathcal{R} \times \begin{cases} \mathcal{H}(\xi, 0) - \frac{\ln \xi}{\xi - 1}, & \xi \neq 1; \\ \mathcal{H}(1, 0) - 1, & \xi = 1, \end{cases} \quad (63)$$

where the function  $\mathcal{H}(\xi, s)$  is given in Appendix C. More generally,  $W_{*g}$  is a finite quantity for the stellar component of J3 models; it follows that it is possible to define the (3-dimensional) stellar virial velocity dispersion as  $\sigma_V^2 = -W_{*g}/M_*$ . Once  $W_{**}$  is known,  $W_{*DM}$  is immediately obtained as  $W_{*g} - W_{**}$ , and we have

$$W_{**} = -4\pi G \int_0^\infty \rho_*(r) M_*(r) r dr = -\frac{\Psi_n M_*}{2}. \quad (64)$$

As well known, in multi component systems the energy  $W$  of a given component is *not* the potential energy of the component itself in the total potential. Therefore, we shall now calculate the different contributions to the potential energy  $U_*$  of the stellar component. As done for the interaction energy  $W_*$ , we can decompose the potential energy  $U_*$  as

$$U_* = U_{*g} + U_{*BH}, \quad (65)$$

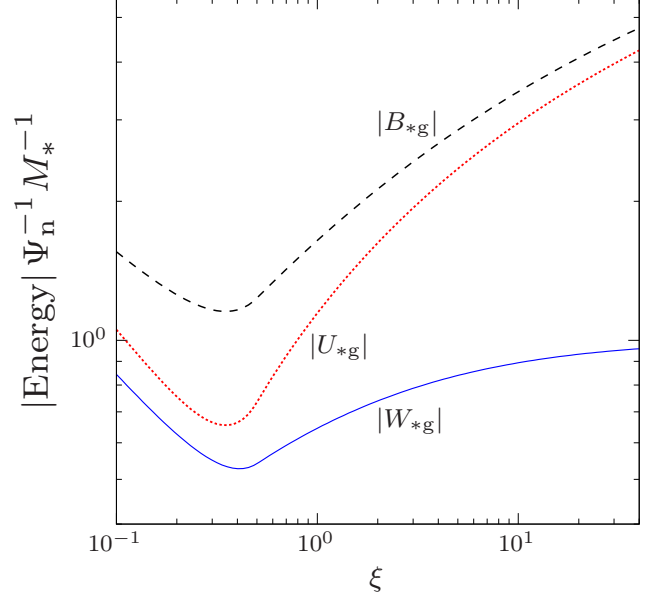


**Figure 6.** Absolute values of the normalized gravitational energies for the stellar component, as a function of  $\xi$ , in case of minimum halo and absence of a central BH. See Sect. 5 for more details.

where

$$U_{*g} = U_{**} + U_{*DM} = \frac{1}{2} \int \rho_* \Phi_* d^3\mathbf{x} + \int \rho_* \Phi_{DM} d^3\mathbf{x}. \quad (66)$$

As well known,

$$U_{*BH} = \int \rho_* \Phi_{BH} d^3\mathbf{x} = W_{*BH}, \quad (67)$$

and so  $U_{*BH}$  diverges as  $W_{*BH}$ . Moreover, the self-gravitational energy and the virial self energy of each density component coincide, and in our case  $U_{**} = W_{**}$ . In order to derive  $U_{*g}$  and  $U_{*DM}$  in eq. (66), we calculate the quantity

$$B_{*g} \equiv \int \rho_* \Phi_g d^3\mathbf{x} = -\Psi_n M_* \mathcal{R} \mathcal{H}(\xi, 0). \quad (68)$$

With this definition one has that  $U_{*g} = B_{*g} - U_{**}$ , and  $U_{*DM} = B_{*g} - 2U_{**}$ . The trends of  $|U_{*g}|$ ,  $|B_{*g}|$ , and  $|W_{*g}|$ , as function of  $\xi$ , are shown in Fig. 6.

Note that  $B_{*g}$  is *not* the gravitational energy  $U_{*g}$  of the stars in the galaxy total potential, but an important quantity in the theory of galactic winds, and in studies of the hot gas content of early-type galaxies. For examples, it measures the energy per unit time ( $L_{grav}$ ) to be provided to the ISM of early-type galaxies (via, e.g., supernova explosions, or thermalization of the velocity of stellar winds, or AGN feedback) in order to steadily extract the mass input injected over the galaxy body from evolving stars. This power is given as  $L_{grav} \propto |B_{*g}|$  (e.g., see Pellegrini 2011, Posacki et al. 2013).

### 5.1 Stability

A particularly relevant application of the VT is in the determination of the conditions required to prevent the onset of the Radial Orbit Instability (hereafter, ROI). Indeed, stellar systems supported by a large amount of radial orbits are in general unstable (e.g., Fridman & Polyachenko 1984, and references therein). As shown by several numerical studies of one and two component systems (see,

e.g., Merritt & Aguilar 1985; Bertin & Stiavelli 1989; Saha 1991, 1992; Bertin et al. 1994; Meza & Zamorano 1997; Nipoti, Londrillo & Ciotti 2002), quantitative information about stability can be obtained by using the function

$$\Xi \equiv \frac{2K_{*r}}{K_{*t}} = -\frac{4}{2 + W_{*g}/K_{*r}}. \quad (69)$$

where  $K_{*r}$  and  $K_{*t} = K_* - K_{*r}$  are the total kinetic energy of stars, associated with the radial and tangential components of the velocity dispersion tensor, respectively (see eq. [60]), and the last expression in eq. (69) derives from eq. (59). Of course, we *exclude* the effect of the central BH, to avoid the divergence of the kinetic energy  $K_{*BH}$ . From its definition,  $\Xi \rightarrow 1$  for  $s_a \rightarrow \infty$  (globally isotropic models), whereas  $\Xi \rightarrow \infty$  for  $s_a \rightarrow 0$  (fully radially anisotropic models). Note that, for  $\mu = 0$ ,  $\Xi$  is independent of  $\mathcal{R}$ . Here we adopt the usual empirical requirement for stability of  $\Xi < 1.70 \pm 0.25$ .

With an analogous treatment to that adopted to derive eq. (54), it can be shown that

$$K_{*r} = 2\pi G \int_0^\infty \mathcal{L}(r) \rho_*(r) M_g(r) \left(1 + \frac{r_a^2}{r^2}\right) dr, \quad (70)$$

where

$$\mathcal{L}(r) = r - r_a \arctg \frac{r}{r_a}, \quad (71)$$

which tends to  $r$  in the limit  $r_a \rightarrow 0$ , in agreement with the VT in eq. (59).

Unfortunately  $K_{*r}$  cannot be expressed via elementary functions, so that we explore numerically the fiducial stability condition  $\Xi(s_a, \xi) = 1.7$ . In Fig. 3 with the green dashed curve we plot the resulting lower bound for stability  $s_a(\xi)$ . The resulting trend, i.e. the fact that  $s_a(\xi)$  increases with  $\xi$ , is in agreement with the behaviour of other families of one and two component models (Ciotti 1996, 1999, CMZ09, CZ18, see also Carollo et al. 1995). As already discussed in CZ18, in order to guarantee the stability of the system, the increase of  $s_a$  with  $\xi$  is a simple consequence of the orbital distribution in OM models, which are radially anisotropic for large  $r$  and isotropic in the central region. Moreover,  $s_a(\xi)$  is quite larger than the critical values  $s_a$  for consistency, so that the maximally radially anisotropic models with positive DF are almost certainly unstable.

## 6 CONCLUSIONS

A new family of spherical, two-component galaxy models is presented, following the approach introduced in CMZ09 and CZ18. These models, called J3 models, have a stellar component described by the Jaffe density profile, and a *total* density component such that the resulting DM halo – defined as the difference between the total and the stellar density distributions – can be made asymptotically identical to a NFW profile, both at the center and at large radii. This property makes the J3 models an improvement over JJ models, while retaining the same analytical simplicity. A BH is also added at the center of the system, and the orbital structure of the stellar component follows the Osipkov-Merritt anisotropy profile. The models are fully determined once the total stellar mass ( $M_*$ ) and its scale length ( $r_*$ ) are assigned, together with a total-to-stellar density ratio ( $\mathcal{R}$ ), a total-to-stellar scale length ratio ( $\xi$ ), a BH-to-stellar mass ratio ( $\mu$ ), and finally the anisotropy radius ( $r_a$ ) of the stellar component. The J3 models allow for an almost complete analytical treatment with quite simple explicit expressions of several

quantities of interest in observational and theoretical works. The main results can be summarized as follows.

- We derive analytical constraints on  $\mathcal{R}$  and  $\xi$  to assure positivity and monotonicity of the DM halo density distribution. For a given  $\xi$ , the model corresponding to the minimum value allowed for  $\mathcal{R}$  is called *minimum halo model*. In particular, for  $\xi \geq 1/2$  the positivity and monotonicity conditions coincide, requiring  $\mathcal{R} \geq \xi$ . For arbitrary choices of  $\mathcal{R}$  and  $\xi$ , near the origin the DM density profile diverges as  $\rho_{DM}(r) \propto r^{-2}$ , but in the minimum halo case with  $\xi > 1/2$  the models are centrally “baryon dominated”, with  $\rho_{DM}(r) \propto r^{-1}$ , as for the NFW profile. Moreover, at large radii  $\rho_{DM}(r)$  is, by construction, always proportional to  $r^{-3}$ , again following the NFW profile. Two simple formulae determine the parameters of the NFW model *identical* to  $\rho_{DM}(r)$  at the center and at large radii; remarkably, the NFW profile so obtained stays close to  $\rho_{DM}(r)$  also in the intermediate region.

- The minimum value of the OM anisotropy radius  $r_a$ , corresponding to a dynamically consistent stellar component, is first estimated using the necessary and sufficient conditions given in CP92. The consistency analysis is then performed for the isotropic DM halo and in presence of a central BH; it is found that for  $\xi \geq 1$ , once *positivity only* of  $\rho_{DM}(r)$  is assured, i.e.  $\mathcal{R} \geq \xi$ ,  $\rho_{DM}$  automatically satisfies the NC and WSC, and so it can be supported by a nowhere negative phase-space DF.

- The DF is then recovered numerically, and we illustrate its behavior for a few representative cases, for different choices of  $\mathcal{R}$ ,  $\xi$ , and  $r_a$ . Then we determined the (minimum) critical value of  $r_a$ , as a function of the model parameters, finding a curve that nicely parallels that given by the WSC. We showed that in absence of the central BH, the minimum value of  $r_a$  depends only on  $\xi$ , and it is independent of  $\mathcal{R}$ . For example, for models with  $\xi = 13$  and no BH, the positivity of the DF requires  $r_a \gtrsim 0.0143 r_*$ . In particular,  $r_a$  decreases for increasing  $\xi$ , i.e., a DM halo more extended than the stellar distribution increases the ability of the stellar component to sustain radial anisotropy. On the contrary, more concentrated DM halos require a more isotropic orbital distribution. This behavior is similar to what already found for JJ models.

- Having determined the region of the parameter space corresponding to physically consistent models, we solved analytically the Jeans equations for the stellar component, for generic values of the model parameters. The asymptotic expansions of  $\sigma_r(r)$  and  $\sigma_p(R)$  near the center and at large radii were obtained; it is shown that J3 models, in the central region, behave identically to JJ models. Accordingly when  $\mu = 0$  and for all values of  $r_a > 0$  (isotropic case included),  $\sigma_p^2(0) = \sigma_r^2(0) = \Psi_n \mathcal{R} / (2\xi)$ . In presence of the BH, in the central regions  $\sigma_r^2(r) \propto r^{-1}$ , and  $\sigma_p^2(R) \sim 2\Psi_n \mu r_*/(3\pi R)$ , independently of  $r_a$ . These results can be used, among other applications, to estimate the size of the so-called “sphere of influence” of the central BH.

- Finally, the analytical expressions for the quantities entering the Virial Theorem, such as the stellar kinetic energy, the interaction energy, and the potential energies, are derived as a function of the model parameters. We also evaluated numerically the minimum value of  $r_a$  corresponding to the fiducial value of  $\simeq 1.7$  for the Friedmann-Poliachenko-Shuckman instability indicator, so that more anisotropic models are prone to the onset of Radial Orbit Instability. The minimum  $r_a$  for stability increases for increasing  $\xi$ , and (in absence of the central BH) its value depends only on  $\xi$ , being independent of  $\mathcal{R}$ .

We conclude by noting that J3 models can be a useful starting point for more advanced modeling of the dynamics of elliptical

galaxies, and can be easily implemented in numerical simulations. In addition, it can be shown that J3 models allow for a fully analytical treatment of Bondi accretion along the lines discussed elsewhere (Ciotti & Pellegrini 2017, 2018); we defer this study to a future work.

## ACKNOWLEDGMENTS

We thank the anonymous referee for useful comments, that improved the presentation.

## REFERENCES

- An J.H., & Evans N.W., 2006, *ApJ*, 642, 752  
 Bertin G., 2000, *Dynamics of Galaxies*, Cambridge University Press  
 Bertin G., & Stiavelli M., 1989, *ApJ*, 338, 723  
 Bertin G., Pegoraro F., Rubini F., & Vesperini E., 1994, *ApJ*, 434, 94  
 Bertin G., Bertola F., Buson L. M., Danzinger I. J., Dejonghe H., Sadler E. M., Saglia R. P., de Zeeuw P. T., Zeilinger W. W., 1994, *A&A*, 292, 381  
 Binney J., & Mamon G., 1982, *MNRAS*, 200, 361  
 Binney J., & Tremaine S., 2008, *Galactic Dynamics*, 2nd Ed. (Princeton University Press, Princeton)  
 Bullock J.S., & Boylan-Kolchin M., 2017, *Annu. Rev. Astron. Astrophys.*, 55, 343  
 Cappellari M., Emsellem E., Bacon R., Bureau M., Davies R. L., de Zeeuw P. T., Falcon-Barroso J., Krajnovic H., Kuntschner H., McDermid R. M., Peletier R. F., Sarzi M., van den Bosch R. C. E., van den Ven G., 2007, *MNRAS*, 379, 418  
 Carollo C. M., de Zeeuw P. T., van der Marel R. P., 1995, *MNRAS*, 276, 1131  
 Ciotti L., 1996, *ApJ*, 471, 68  
 Ciotti L., 1999, *ApJ*, 520, 574  
 Ciotti L., 2000, *Lecture Notes on Stellar Dynamics* (Pisa: Scuola Normale Superiore Ed.)  
 Ciotti L., & Lanzoni B., 1997, *A&A*, 321, 724  
 Ciotti L., & Morganti L., 2009, *MNRAS*, 393, 179  
 Ciotti L., & Morganti L., 2010a, *MNRAS*, 401, 1091  
 Ciotti L., & Morganti L., 2010b, *MNRAS*, 408, 1070  
 Ciotti L., & Pellegrini S., 1992, *MNRAS*, 255, 561 (CP92)  
 Ciotti L., & Pellegrini S., 2017, *ApJ*, 848, 29  
 Ciotti L., & Pellegrini S., 2018, *ApJ*, 868, 91  
 Ciotti L., Morganti L., de Zeeuw P. T., 2009, *MNRAS*, 393, 491 (CMZ09)  
 Ciotti L., & Ziaee Lorzad A., 2018, *MNRAS*, 473, 5476 (CZ18)  
 Czoske O., Barnabe M., Koopmans L. E. V., Treu T., Bolton A. S., 2008, *ApJ*, 384, 987  
 de Bruijn Jos H. J., van der Marel R. P., de Zeeuw P. T., 1996, *MNRAS*, 282, 909  
 Dehnen W., 1993, *MNRAS*, 265, 250  
 De Vaucouleurs G., 1948, *Ann.Astr.*, 11, 247  
 Dye S., Evans N. W., Belokurov V., Warren S. J., Hewett P., 2008, *MNRAS*, 388, 384  
 Fridman A. M., & Polyachenko V. L., 1984, *Physics of Gravitating Systems* (Springer, New York)  
 Gavazzi R., Treu T., Rhodes J. D., Koopmans L. V. E., Bolton A. S., Burles S., Massey R. J., Moustakas L. A., 2007, *ApJ*, 667, 176  
 Gerhard O., Kronawitter A., Saglia R. P., Bender R., 2001, *AJ*, 121, 1936  
 Gradshteyn I. S., Ryzhik I. M., 2007, in Jeffrey A., Zwillinger D. E., eds, *Table of Integrals, Series, and Products*, 7th edn. Elsevier, Amsterdam  
 Hiottelis N., 1994, *A&A*, 291, 725  
 Jaffe W., 1983, *MNRAS*, 202, 995  
 Kochanek C. S., 1994, *ApJ*, 436, 56  
 Kormendy J., & Ho L. C., 2013, *ARA&A*, 51, 511  
 Lewin L., *Polylogarithms and Associated Functions*, 1981, New York: North-Holland  
 Magorrian J., Tremaine S., Richstone D., et al., 1998, *AJ*, 115, 2285  
 Merritt D., 1985, *AJ*, 90, 1027  
 Merritt D., & Aguilar L. A., 1985, *MNRAS*, 217, 787  
 Meza A., & Zamorano N., 1997, *AJ*, 490, 136  
 Naab T., & Ostriker J. P., 2007, *MNRAS*, 366, 899  
 Navarro J. F., Frenk C. S., White S. D. M., 1997, *ApJ*, 490, 493  
 Nipoti C., Londrillo P., & Ciotti L., 2002, *MNRAS*, 332, 901  
 Nipoti C., Treu T., & Bolton A. S., 2008, *MNRAS*, 390, 349  
 Osipkov L. P., 1979, *Pis'ma Astron. Zh.*, 5, 77  
 Pellegrini S., 2011, *ApJ*, 738, 57  
 Posacki S., Pellegrini S., & Ciotti L., 2013, *MNRAS*, 433, 2259  
 Rix H. W., de Zeeuw P. T., Cretton N., van der Marel R. P., Carollo C. M., 1997, *ApJ*, 488, 702  
 Saha P., 1991, *MNRAS*, 148, 494  
 Saha P., 1992, *MNRAS*, 254, 132  
 Shankar F., et al., 2017, *ApJ*, 840, 34  
 Stiavelli M., & Sparke L. S., 1991, *ApJ*, 382, 466  
 Tremaine S., et al., 1994, *AJ*, 107, 634  
 Treu T., & Koopmans L. V. E., 2002, *ApJ*, 575, 87  
 Treu T., & Koopmans L. V. E., 2004, *ApJ*, 611, 739  
 van den Bosch R. C. E., van de Ven G., Verolme E. K., Cappellari M., de Zeeuw P. T., 2008, *MNRAS*, 385, 647  
 van Hese E., Baees M., Dejonghe H., 2011, *ApJ*, 726, 80

## APPENDIX A: PROJECTED DENSITIES

For the stellar density, the functions  $f_*(\eta)$  and  $g_*(\eta)$  appearing in eqs. (4) and (6) are given by

$$f_*(\eta) = \begin{cases} \frac{1}{4\eta} + \frac{\sqrt{1-\eta^2} - (2-\eta^2) \operatorname{arcsech} \eta}{2\pi(1-\eta^2)^{3/2}}, & 0 < \eta < 1, \\ \frac{1}{4} - \frac{2}{3\pi}, & \eta = 1, \\ \frac{1}{4\eta} - \frac{\sqrt{\eta^2-1} + (\eta^2-2) \operatorname{arcsec} \eta}{2\pi(\eta^2-1)^{3/2}}, & \eta > 1, \end{cases} \quad (\text{A1})$$

and

$$g_*(\eta) = \eta \times \begin{cases} \frac{\pi}{2} - \eta \frac{\operatorname{arcsech} \eta}{\sqrt{1-\eta^2}}, & 0 < \eta < 1, \\ \frac{\pi}{2} - 1, & \eta = 1, \\ \frac{\pi}{2} - \eta \frac{\operatorname{arcsec} \eta}{\sqrt{\eta^2-1}}, & \eta > 1, \end{cases} \quad (\text{A2})$$

where  $\eta = R/r_*$ . For the total galaxy density, the analogous functions  $f_g(\eta)$  and  $g_g(\eta)$  appearing in eqs. (9) and (11) read

$$f_g(\eta) = \begin{cases} \frac{1}{4\eta} - \frac{\operatorname{arcsech} \eta}{2\pi\sqrt{1-\eta^2}}, & 0 < \eta < 1, \\ \frac{1}{4} - \frac{1}{2\pi}, & \eta = 1, \\ \frac{1}{4\eta} - \frac{\operatorname{arcsec} \eta}{2\pi\sqrt{\eta^2-1}}, & \eta > 1, \end{cases} \quad (\text{A3})$$

and

$$g_g(\eta) = \eta \times \begin{cases} \frac{\pi}{2} - \frac{\ln(2/\eta)}{\eta} + \frac{\sqrt{1-\eta^2} \operatorname{arcsech} \eta}{\eta}, & 0 < \eta < 1, \\ \frac{\pi}{2} - \ln 2, & \eta = 1, \\ \frac{\pi}{2} - \frac{\ln(2/\eta)}{\eta} - \frac{\sqrt{\eta^2-1} \operatorname{arcsec} \eta}{\eta}, & \eta > 1, \end{cases} \quad (\text{A4})$$

where now  $\eta = R/r_g$ .

**APPENDIX B: POSITIVITY AND MONOTONICITY OF THE DARK MATTER HALO**

The condition for the *positivity* of the DM halo density is obtained by imposing  $\rho_{\text{DM}}(r) \geq 0$ , i.e.

$$\mathcal{R} \geq \frac{\xi + s}{(1 + s)^2}, \quad s \geq 0. \quad (\text{B1})$$

Therefore, in order to have a nowhere negative DM halo for given  $\xi$ ,  $\mathcal{R}$  must be greater than or equal to the maximum  $\mathcal{R}_m(\xi)$  of the function above, and simple algebra proves eq. (16).

The *monotonicity* condition for  $\rho_{\text{DM}}$  is then obtained by requiring that  $d\rho_{\text{DM}}(r)/dr \leq 0$ , i.e.

$$\mathcal{R} \geq \frac{2(\xi + s)^2(1 + 2s)}{(1 + s)^3(2\xi + 3s)} \equiv \mathcal{M}(\xi, s), \quad s \geq 0, \quad (\text{B2})$$

and by the same argument as above, we call  $\mathcal{R}_{\text{mon}}(\xi)$  the maximum of the function  $\mathcal{M}(\xi, s)$ . We obtain

$$\frac{d\mathcal{M}(\xi, s)}{ds} \propto (1 - 2\xi)[\xi + (3 + 4\xi)s] + 6(1 - 3\xi)s^2 - 6s^3, \quad (\text{B3})$$

where proportionality indicates product by a strictly positive function. The explicit solution of eq. (B3) presents no difficulty, however important information can be easily obtained without solving it. First, for  $\xi \geq 1/2$  eq. (B3) is nowhere positive, and so the maximum of  $\mathcal{M}$  is reached at the center, with  $\mathcal{R}_{\text{mon}}(\xi) \equiv \mathcal{M}(\xi, 0) = \xi = \mathcal{R}_m(\xi)$ . In practice, for  $\xi \geq 1/2$  the *positivity and monotonicity conditions coincide*, similarly to the case of JJ models, where the positivity and monotonicity conditions coincide for all values of  $\xi$ . For  $0 < \xi < 1/2$  the situation is different. In fact, the cubic function in eq. (B3) is positive for small values of  $s$ , and negative for large values of  $s$ , and so  $d\mathcal{M}(\xi, s)/ds$  has at least one zero (and  $\mathcal{M}$  at least one maximum) for  $s \geq 0$ . Moreover, the Descartes Theorem shows that for  $0 < \xi < 1/2$  at most one positive zero of the cubic exists, therefore corresponding to the single maximum  $\mathcal{R}_{\text{mon}}(\xi)$ : as we are mainly interested in realistic models with  $\xi \geq 1$ , we do not discuss further this case.

As illustrated in Sect. 3.1, for an isotropic DM halo the NC is equivalent to the monotonicity of the density profile, and from the results obtained above, for  $\xi \geq 1/2$  positivity, monotonicity and NC coincide, and hold for  $\mathcal{R} \geq \xi$ . The WSC for the isotropic halo in the total galactic potential and in *absence* of the central BH involves a cumbersome function, and so we do not give here its expression: a numerical study indicates however that for  $\xi \geq 1$  the WSC holds when  $\mathcal{R} \geq \xi$ . The WSC for the isotropic halo in the potential of a dominant central mass reduces to

$$\mathcal{R} \geq \frac{(\xi + s)^3(6s^2 + 4s + 1)}{(1 + s)^4(3s^2 + 3\xi s + \xi^2)}, \quad (\text{B4})$$

and simple algebra shows that for  $\xi \geq 1$  the maximum is reached at  $s = 0$ , i.e. again for  $\mathcal{R} \geq \xi$ . Therefore, from the discussion after eq. (30) we conclude that for  $\xi \geq 1$  and  $\mathcal{R} \geq \xi$  the WSC for the isotropic DM halo with a central BH of arbitrary mass holds.

As for the halo, also for the Jaffe stellar distribution the WSC leads to an analytical but cumbersome expression. In absence of the central BH ( $\mu = 0$ ) the WSC reduces to

$$s_a^2 \geq - \frac{s^3[(\xi + s)(s - 2)\ln(1 + s/\xi) + s(1 + s)]}{(\xi + s)(6s^2 + 4s + 1)\ln(1 + s/\xi) + s(1 + s)(1 + 2s)}, \quad (\text{B5})$$

for  $s \geq 0$ , where it can be noticed that the parameter  $\mathcal{R}$  does not appear. The result of the numerical investigation of the inequality above is represented by the red dotted line in Fig. 3, where we show the minimum value  $s_a^-(\xi)$ .

**APPENDIX C: THE FUNCTION  $\mathcal{H}(\xi, s)$** 

The function  $\mathcal{H}$  is defined as

$$\mathcal{H}(\xi, s) \equiv \int_s^\infty \ln\left(1 + \frac{1}{t}\right) \frac{dt}{\xi + t} = \text{Li}_2\left(\frac{1}{1 + s}\right) + \begin{cases} \frac{1}{2} \ln \frac{1 + s}{\xi + s} \ln \frac{(1 - \xi)^2(1 + s)}{\xi + s} + \text{Li}_2\left[\frac{\xi(1 + s)}{\xi + s}\right] - \text{Li}_2(\xi), \\ 0, \\ \ln \frac{\xi}{\xi - 1} \ln \frac{\xi + s}{1 + s} - \text{Li}_2\left[\frac{\xi + s}{\xi(1 + s)}\right] + \text{Li}_2\left(\frac{1}{\xi}\right), \end{cases} \quad (\text{C1})$$

where the three expressions (that can be obtained with some work starting from the change of variable  $1 + t = 1/y$ ) refer to  $0 < \xi < 1$ ,  $\xi = 1$ , and  $\xi > 1$ , respectively, and

$$\text{Li}_2(x) = - \int_0^x \frac{\ln(1 - t)}{t} dt, \quad x \leq 1, \quad (\text{C2})$$

is the dilogarithm function (e.g., Gradshteyn & Ryzhik 2007, see also Lewin 1981), with the Euler identity  $\text{Li}_2(1) = \pi^2/6$ . At the center,

$$\mathcal{H}(\xi, 0) = \begin{cases} \frac{\pi^2}{3} + \frac{(\ln \xi)^2}{2} - \ln \xi \ln(1 - \xi) - \text{Li}_2(\xi), \\ \frac{\pi^2}{6}, \\ (\ln \xi)^2 - \ln \xi \ln(\xi - 1) + \text{Li}_2\left(\frac{1}{\xi}\right), \end{cases} \quad (\text{C3})$$

while a direct expansion of eq. (C1) proves that

$$\mathcal{H}(\xi, s) = \begin{cases} \mathcal{H}(\xi, 0) + \frac{s \ln s}{\xi} + \mathcal{O}(s), \\ \frac{1}{s} - \frac{2\xi + 1}{4s^2} + \mathcal{O}\left(\frac{1}{s^3}\right), \end{cases} \quad (\text{C4})$$

for  $s \rightarrow 0$  and  $s \rightarrow \infty$ , respectively.